

Superconducting Bi-Ca-Sr-Cu-O Fibers Grown by the Laser-Heated Pedestal Growth Method

R. S. FEIGELSON, D. GAZIT,* D. K. FORK, T. H. GEBALLE

Superconducting fibers of several compositions including the nominal composition $\text{Bi}_2\text{CaSrCu}_2\text{O}_8$ have been grown by means of the laser-heated pedestal growth method. The influence of starting composition and growth conditions on structure and superconducting properties is discussed. The a - b planes of the material are parallel to the fiber axis (along the growth direction), providing the ideal condition for conduction along the copper-oxygen planes.

THE LASER-HEATED PEDESTAL GROWTH (LHPG) method has been shown to be a powerful method for rapidly growing small-diameter single crystals, particularly oxides, both for measurements of properties and for fabricating fiber devices (1, 2). It is a containerless technique that does not require a conventional furnace and can be used to grow crystals of very high melting-temperature materials without worry about reactivity with components in the growth system. It characteristically involves steep axial temperature gradients that permit rapid growth rates (typically millimeters per minute) and high quench rates that have made possible the growth of crystals of metastable compounds such as the high-temperature hexagonal form of BaTiO_3 (2). The sharply focused laser beam permits the formation of narrow molten zones that allow the growth of single-crystal fibers of micrometer diameter.

Following the early work by Burrus and Stone (3), an extensive program has been undertaken at Stanford that has produced a large number of different types of single-crystal fibers. Following the discovery of high-temperature superconducting transitions in the copper oxide perovskite systems by Bednorz and Müller (4), it seemed worthwhile to attempt to grow single-crystal fibers of the high transition temperature (T_c) materials for a number of reasons. There is evidence that fiber single crystals can be the most perfect crystals that are grown by any means. With the proper choice of seed, fibers of different orientations can be grown, a particularly valuable attribute if it can be done for the highly

anisotropic layered copper oxide superconductors. Also, oxide fibers have been grown small enough in cross section to be flexible and thus have the possibility to serve as model systems for making the superconductors in wire form. Finally, the LHPG technique is closely related to the float-zone method, which is known to be the best technique for growing incongruently melting compositions.

Since all the new high T_c superconducting phases exhibit complex incongruent melting behavior, it was suggested (5) that the LHPG technique should be ideally suited to the growth of these materials in fiber form. One of the major advantages of this method is that an a priori knowledge of the actual melt composition required to produce the appropriate steady state growth conditions is not needed. The melt automatically adjusts itself to exactly the right composition needed, as demanded by the thermodynamic properties of the system.

Initial attempts with the $(\text{LaSr})_2\text{CuO}_4$ and $\text{YBa}_2\text{Cu}_3\text{O}_7$ compounds were not successful owing to decomposition and loss of CuO. Even though some superconductivity was obtained, it was evident that in order to obtain the desired composition and single-crystal structure it would be necessary to enrich the feed stock with CuO. With the discovery of high T_c in the Bi-Ca-Sr-Cu-O system (6) and its stability with respect to oxygen (7), it became worthwhile to investigate the applicability of the LHPG method to the growth of these new compounds. In this report the preparation, structure, and some of the superconducting properties of dense, oriented, large-grain polycrystalline fibers grown from $\text{Bi}_2\text{CaSr}_2\text{Cu}_2\text{O}_{8-\delta}$ and $\text{Bi}_{1.8}\text{Ca}_{1.2}\text{Sr}_{1.8}\text{Cu}_{2.2}\text{O}_{8-\delta}$ starting materials will be discussed.

A schematic of the LHPG method is given in Fig. 1, top. The top of the source rod of the material to be grown is melted

with a tightly focused laser beam ($\sim 50 \mu\text{m}$ wide) having a circular cross section. A seed crystal is then introduced into the melt and growth is accomplished by withdrawing the seed at a controlled rate. To maintain constant melt volume the source rod is fed into the laser beam at a rate determined by the fiber diameter desired.

The source material in these experiments was prepared from Bi_2O_3 , CaCO_3 , SrCO_3 , and CuO powders. The appropriate amounts were mixed together, finely ground, pressed into a pellet, and sintered for 15 hours in air at 780°C . The pellet was then ground, pressed again, and sintered under the same conditions. Rectangular rods 1.2 by 1.2 by 20 mm in size were cut out of the polycrystalline pellet and used both as the source material and for seeds.

Four different starting compositions were

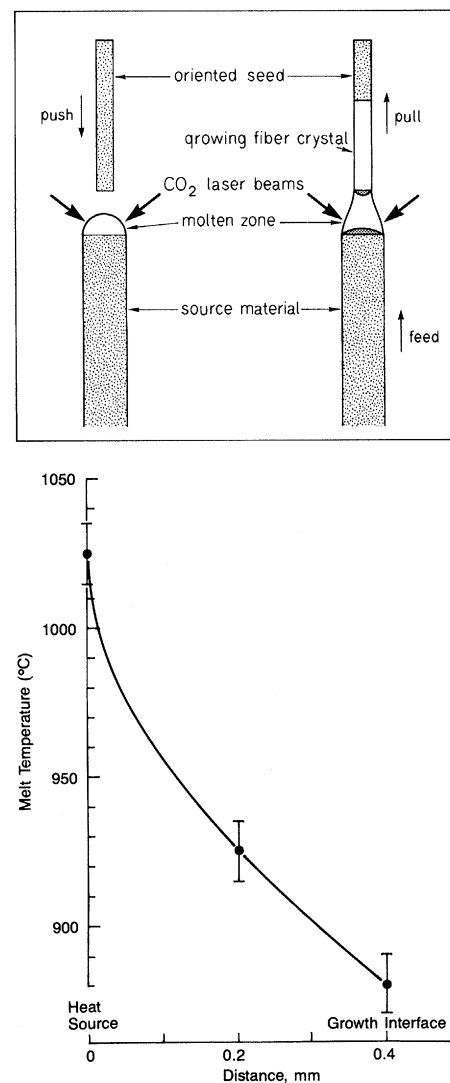


Fig. 1. (Top) Schematic diagram of the laser-heated pedestal growth method. (Bottom) Variation in surface melt temperature as a function of axial distance from the growth interface to the laser contact point. Error limits represent measurement variations over five experiments.

Center for Materials Research and the Department of Applied Physics, Stanford University, Stanford, CA 94305.

*On leave from the Nuclear Research Center Negev, P.O. Box 9001, Beer Sheva, Israel.

Table 1. Details of the different fiber growth runs. The temperatures are uncorrected optical pyrometer values of the melt temperature at the surface near the growth interface. Fiber 3 exhibited a significantly higher resistivity than fibers grown in air or oxygen.

Fiber type	Starting composition Bi-Ca-Sr-Cu	Growth rate (mm/hour)	Diameter (mm)	Atmosphere	Temperature (°C)
1	2-1-2-2	4.8	1.0	Air	900
2	2-1-2-2	1.5	1.0	Air	900
3	2-1-2-2	4.8	1.0	Argon	800
4	2-1-2-2	4.8	1.0	Oxygen	910
5	1.8-1.2-1.8-2.2	4.8	1.0	Air	900
6	1.8-1.2-1.8-2.2	24.0	0.25-0.35	Air	900
7	1.8-1.2-1.8-2.2	4.8	0.25-0.35	Air	900
8	1-1-1-2	4.8	1.0	Air	900
9	2-1-1-3	4.8	1.0	Air	860

used as listed in Table 1. Two different fiber diameters and lengths were grown from the randomly oriented polycrystalline seeds: 1 mm in diameter, 10 to 12 mm in length and 0.25 to 0.35 mm in diameter and 30 to 40 mm long. Different growth conditions were used for the 1 mm fibers as listed in Table 1. The long thin fibers were grown from melts of the first two compositions in air by means of a two-step procedure. In the first step, 0.7 mm diameter fibers were grown with a manually controlled pull rate that was more rapid than that used later. In the second step, two fibers were grown to their final diameter with pull rates of 24.0 and 4.8 mm/hour, respectively. The two-step procedure was used because the molten zone can become unstable when the ratio of the fiber

diameter to the source rod diameter is too small (3). The growth rates used for these compounds, as expected, were lower than those required for congruently melting compounds. The approximate liquidus temperatures near the growth interface were measured during growth using a fine-filament optical pyrometer. Measurements were taken once every 20 to 30 minutes. A plot of the axial temperature gradient is given in Fig. 1, bottom. The temperature during growth was observed to remain constant to within the accuracy of the pyrometer reading. The melt temperature at the growth interface decreased dramatically from 900° to 800°C when an argon atmosphere was introduced into the growth chamber, indicating a strong influence of O₂ partial pressure on melt composition. It changed rapidly back to 900°C when air was reintroduced into the system. The fiber grown in argon had a much higher resistivity than the other fibers. Growth in pure oxygen caused the melt to boil. On replacing the oxygen with air, the boiling stopped immediately. All of

the fibers were black, with varying degrees of surface smoothness except for the fiber which was grown in argon, which had a blackish-copper color.

The surface structure of the 1-mm diameter fiber grown at 4.8 mm/hour (fiber 1, Table 1) had, as shown in Fig. 2, top, a fibrous appearance owing to numerous facets and growth ridges aligned parallel to the growth direction. Figure 2, bottom, shows a fractured cross section of this fiber that clearly reveals the presence of plate-like crystallites having a highly aligned morphology. All of the plates were elongated along the growth direction. The thinner fiber grown at 24 mm/hour (fiber 6, Table 1) had similar structure but with fewer grains. The surface of the more slowly grown (fiber 7, Table 1) fibers (4.8 mm/hour), however, alternated between highly faceted regions like the previous fibers, and smooth regions. These smooth fiber sections developed gradually, eventually extending to the entire circumference as shown in Fig. 3. These smooth regions always ended abruptly, which suggests that their termination was the result of a dynamical growth instability. Uniform scanning electron microscopy (SEM) backscatter results on the smooth surface of the fiber indicated that the surface composition was homogeneous throughout large areas. The cross section of fiber 1 was composed of oriented platelets (grey), surrounded by a

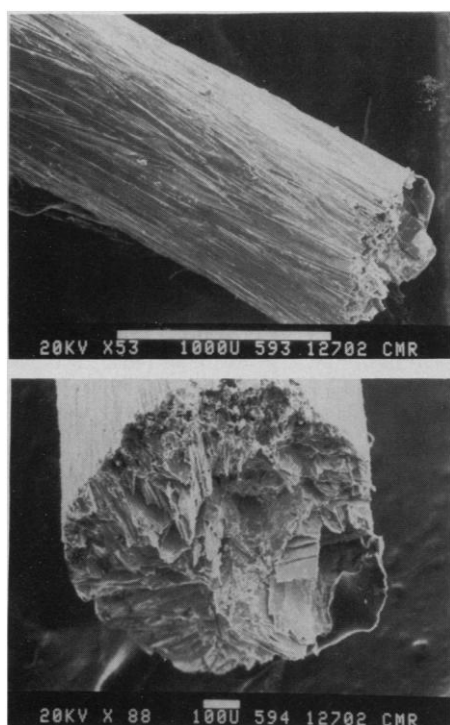


Fig. 2. SEM photographs of 1-mm-diameter Bi₂CaSr₂Cu₂O₈₋₈ fiber grown at 4.8 mm/hour. (Top) Side view. (Bottom) Fractured cross section.

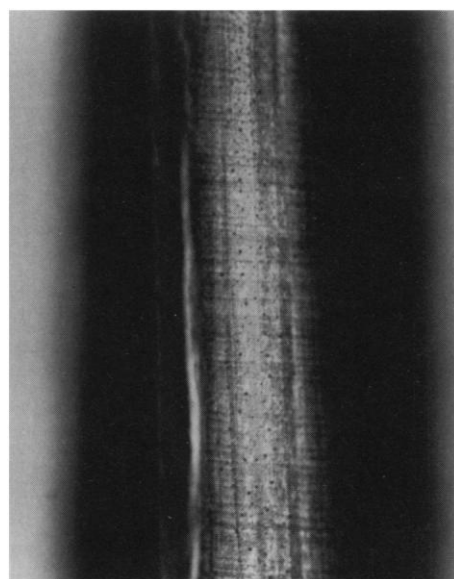


Fig. 3. Optical photograph of a smooth section of Bi_{1.8}Ca_{1.2}Sr_{1.8}Cu_{2.2}O₈₋₈ fiber.

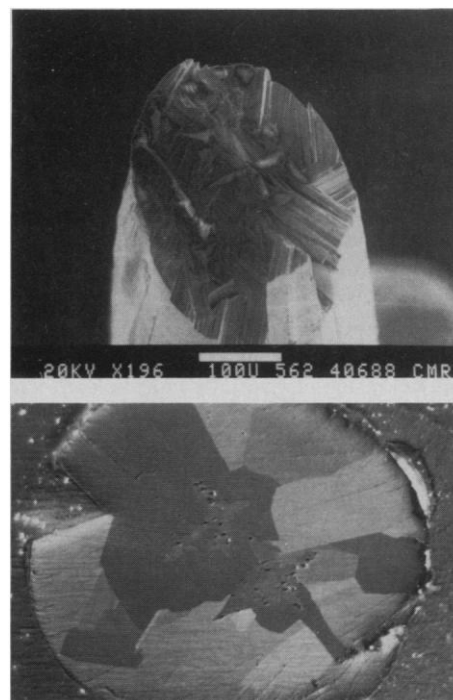


Fig. 4. (Top) SEM photograph of a fractured cross section of Bi_{1.8}Ca_{1.2}Sr_{1.8}Cu_{2.2}O₈₋₈ fiber. (Bottom) Optical photomicrograph of a polished cross section of the same fiber. Both pictures reveal a star-shaped second phase in the core region.

Fig. 5. (Left) X-ray diffraction data for a smooth section of fiber 7. The fiber axis is directed normal to the plane of the x-rays. **(Right)** Powder x-ray diffraction data for fiber 1. The predominance of the c -axis peaks may be due to a tendency for the crystal to cleave along the a - b plane, resulting in small crystals that lie flat with their c -axes directed upward. The powder was ground with a mortar and pestle. All of the $[00n]$ peaks correspond to a c -axis spacing of 30.8 Å.

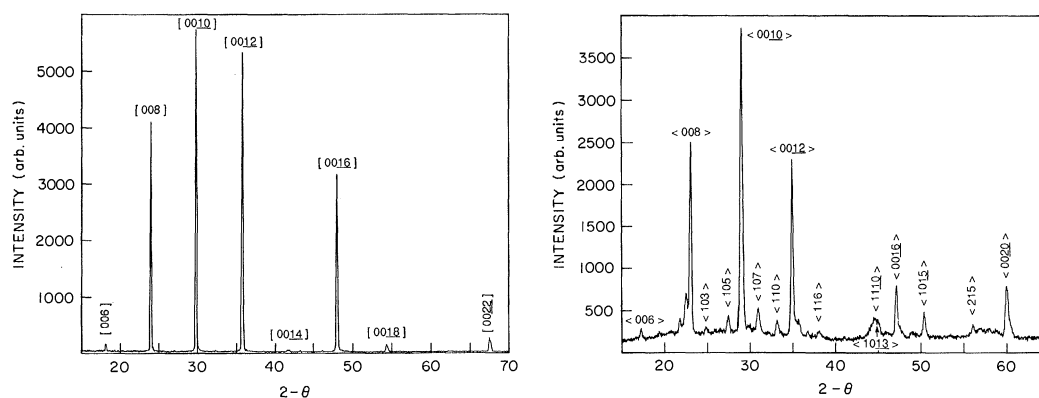
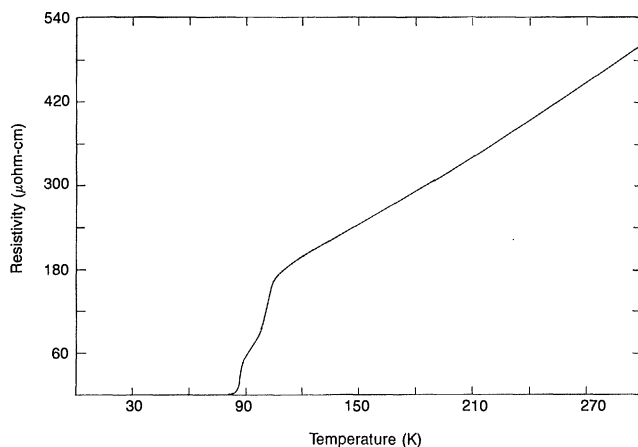


Fig. 6. Resistivity versus temperature for a smooth section of fiber 7.



white matrix phase (~10% by volume). A few tiny dark spots appeared in the microstructure that might be voids or inclusions. Microprobe analysis showed that the grey phase had approximately the 2-1-2-2 composition, whereas the white phase had a variable composition always higher in Bi. The apparent absence of a phase with a circular morphology in the cross section or on the surface led us to the conclusion that the nonsuperconducting needle-like phase usually seen in conventionally melted samples was not formed during the fiber growth experiments. An SEM photograph of the fractured end of a smooth section of fiber is shown in Fig. 4, top. The morphology here is quite different from that seen previously. In these regions several large crystallites cover the entire cross sectional area as can clearly be seen in the photograph of a polished surface given in Fig. 4, bottom. A second phase, in the form of two star-shaped regions near the fiber core, can also be seen. They contain almost pure CaO.

X-ray diffraction measurements were made on a four-circle diffractometer by means of a $\text{CuK}\alpha$ source in the Bragg-Brentano geometry. Five types of x-ray scans were used to verify that the c -axis of the crystallites was perpendicular to the fiber's growth axis. The c -axis $[00n]$ peaks were observed in the smooth fiber section when

the plane containing the incident and scattered x-rays was normal to the fiber. Rocking the fiber toward the plane of the x-rays while tuned to the $[00\bar{1}0]$ peak indicated that the c -axis lies in the cross section to within ~4 degrees. Rotating the fiber about its axis while tuned to the $[0010]$ peak revealed several sharp peaks corresponding to individual c -axis grains in the cross section of the fiber. This result agrees well with the grain structure observed in the SEM photographs of this fiber (Fig. 2). No c -axis-oriented grains were found coaxial with the fiber. Preliminary results indicate that the axial orientation is the $[110]$ direction. The results above were corroborated by placing the fiber axis in the plane of the x-rays and rocking on the c -axis peaks. The same series of x-ray measurements was tried on a rough section of a faster grown thin fiber. These data also revealed crystallites however, much weaker scattering (1.5 orders of magnitude) was observed, suggesting that the crystallites were smaller, and perhaps mixed with other phases. Measurements on the thicker fibers also showed the c -axis normal to the fiber axis. Grain size seems to be inversely related to growth rate for the growth conditions used in these experiments. It is natural to conclude that the direction of slowest growth is the c -

direction.

Figure 5, left, shows the 2θ scan on a smooth section of fiber 7 with the axial direction normal to the plane of the x-rays. The $[00n]$ peaks are visible against an almost flat background. Figure 5, right, shows a powder diffraction pattern made from one of the thicker fibers (fiber 1). When corrections are made for a misalignment in the diffractometer, both sets of diffraction patterns indicate a c -axis spacing of 30.8 Å, in agreement with data (7) for the 85 K (2-1-2-2) phase of the Bi-Ca-Sr-Cu-O materials. Powder diffraction was used for the thick fiber to increase the signal strength.

The resistivity of the samples was measured with the four-point probe technique. Contacts were made with either silver paint or silver epoxy that was later covered with pressed indium. The contact resistance for these contacts was measured to be as high as 350 mohm/cm². The accuracy of the resistivities that we measured was limited by the geometrical factors of cross section and contact spacing. To within orders of unity we could compare the effects of growth and annealing conditions.

The results for the smooth section of fiber 7 show a normal state resistivity which is linear in T and extrapolates to zero at 0 K (Fig. 6). These data were obtained from the same fiber that was photographed in cross section in Fig. 4, bottom, and that produced the diffraction pattern in Fig. 5, left. The two drops in resistivity at 105 K and 85 K as originally observed by Maeda *et al.* (6) are believed to correspond to two superconducting phases of the Bi-Ca-Sr-Cu-O system. Also noted is a very shallow resistance tail in the transition between 85 K and 80 K, which we believe is a sign of percolation between crystallites in the smooth section.

It has been established that in the related system $\text{Tl}_2\text{Ca}_{n-1}\text{Ba}_2\text{Cu}_n\text{O}_{4+2n}$, three different T_c phases with $n = 1, 2, 3$ exist and correspond to critical temperatures of 80 K, 105 K, and 125 K, respectively (8). The 105 K drop in resistivity in Fig. 6 is thus suspected to be the result of a minority phase of

$\text{Bi}_2\text{Ca}_2\text{Sr}_2\text{Cu}_3\text{O}_{10}$, whose unit cell includes an extra copper-oxygen layer. Tsuchiya *et al.* (9) have presented cross-sectional transmission electron microscopy results of double, triple, and quadruple copper-oxygen layers in the Bi-Ca-Sr-Cu-O systems.

None of the remaining samples, with one exception, had either a linear resistance extrapolating to zero or a pair of two superconducting transitions. To obtain superconducting transitions for the narrow diameter nonsmooth fibers, it was necessary to anneal them in air at 500°C, in contrast to the data in Fig. 6, which were obtained for an unannealed portion of the smooth fiber. This suggests that the process that forms the large oriented crystallites in the smooth fiber sections also accompanies the incorporation of adequate quantities of oxygen. The results thus indicate that an oxygen anneal lowers the resistivity and narrows the superconducting transition of the thick fibers, as well as the rough portions of thin fibers.

It is of great interest to measure the critical currents of the fibers and, following the work by Elkin *et al.* (10) on YBCO, improved contacts on the fibers have been made by ion milling the surface and depositing silver or gold contacts on the surface. With a pressed indium overlayer, these contacts had resistivities of 30 to 40 $\mu\text{ohm}/\text{cm}^2$, but the critical current measurements are not yet complete.

We have demonstrated a capability for growing, under controlled conditions, superconducting fibers by means of the laser-heated pedestal growth technique. Under the right conditions, the growth process leads to several simultaneously occurring properties which make them ideal for study. The *a-b* planes are directed along the axis of the fiber, which we believe optimizes conduction in the axial direction. A reduced number of larger crystallites takes over during the growth of the smooth sections, which should augment the critical current. The fiber's surface morphology becomes smooth, facilitating the placement of electrical contacts. The superconducting transition consists of two distinct drops which we believe results from a phase with higher T_c .

Note added in proof: Preliminary measurements (11) with a pulsed current showed an excess of 60,000 A/cm² at 68 K.

REFERENCES AND NOTES

1. R. S. Feigelson, in *Crystal Growth of Electronic Materials*, E. Kaldis, Ed. (North-Holland, Amsterdam, 1985), pp. 127-145; in *Tunable Solid State Lasers*, P. Hammerling, A. B. Budgor, A. Pinto, Eds. (Springer, New York, 1985), pp. 129-141.
2. ———, *J. Crystal Growth* 79, 669 (1986).
3. C. A. Burrus and J. Stone, *Appl. Phys. Lett.* 26, 318 (1974).
4. J. Bednorz and K. A. Müller, *Z. Phys. B* 64, 189 (1986).
5. R. S. Feigelson and Y. X. Fan, paper presented at the

- Seventh American Conference on Crystal Growth, 12 to 17 July 1987, Monterey, CA.
6. H. Maeda, Y. Tanaka, M. Fukutomi, T. Asano, *Jpn. J. Appl. Phys.* 27, L209 (1988).
7. See, for example: J. M. Tarascon *et al.*, *Phys. Rev. B*, in press; S. A. Sunshine *et al.*, *ibid.*, in press.
8. See, for example: R. M. Hazen *et al.*, *Phys. Rev. Lett.*, 60, 1174 (1988); S. S. Parkin *et al.*, *ibid.*, in press; C. C. Torardi *et al.*, *Science* 240, 631 (1988).
9. J. Tsuchiya *et al.*, in preparation.
10. J. W. Elkin, A. J. Panson, B. A. Blankenship, *Appl. Phys. Lett.* 52, 331 (1988).
11. J. Sun, D. Fork, A. Kapitulnik *et al.*, private commu-

nications.

12. We thank R. Raymakers for making the polycrystalline starting material, C. B. Eom for assistance with the SEM photographs, J. Sun for preliminary resistivity measurements, R. Barton for useful discussions, S. Ladderman for verifying the diffraction techniques, and M. Lee for assistance in making the contacts. This work was supported by the NSF Materials Research Laboratory program through the Center for Materials Research at Stanford University.

27 April 1988; accepted 5 May 1988

Low Lake Stands in Lakes Malawi and Tanganyika, East Africa, Delineated with Multifold Seismic Data

C. A. SCHOLZ AND B. R. ROSENDAHL

Seismic data reveal that water level in Lake Malawi, East Africa, was 250 to 500 meters lower before about 25,000 years ago. Water levels in Lake Tanganyika at that time were more than 600 meters below the current lake level. A drier climate appears to have caused these low stands, but tectonic tilting may also have been a contributing factor in Lake Malawi. High-angle discordances associated with shallow sequence boundaries suggest that these low stands probably lasted many tens of thousands of years. Because of its basement topography, the Lake Tanganyika basin had three separate paleolakes, whereas the Lake Malawi basin had only one. The different geographies of these paleolakes may be responsible in part for the differences in the endemic fish populations in these lakes.

WE HAVE USED 24-FOLD COMMON depth point seismic reflection data (1) to delineate the boundaries of the predecessors to Lakes Malawi and Tanganyika, East Africa (Figs. 1 and 2). Mapping of paleoshorelines lying many hundreds of meters below modern lake levels is necessary for examining depositional processes in rifts, the limnology and ichthyology of African rift lakes, and the paleoclimatology of East Africa.

Lake Malawi and Lake Tanganyika occupy the southern and central parts of the western branch of the East African rift system (Fig. 1). They are among the world's deepest lakes, and both lie in a region of savannah and subtropical forest (2-5). Structurally, both rifts are composed of a series of linked half-grabens, which tend to have alternating directions of asymmetry along the rift axes (6). Modern depocenters coincide with the most subsided parts of these half-grabens. Multifold seismic data (Fig. 2, A and C) indicate that 4 km or more of sediment have accumulated in the northern basins of the Lake Malawi rift (7) and over 6 km of sediment fill parts of the Lake Tanganyika rift (8, 9).

Several seismic sequence boundaries (10) have been identified in the sediments be-

neath the main African rift lakes (7, 8, 11, 12). These boundaries are major breaks in the lacustrine stratigraphy and represent depositional changes that were caused by climatic, tectonic, and, in the case of the eastern rift (13), volcanogenic processes. The stratigraphic record of abrupt changes

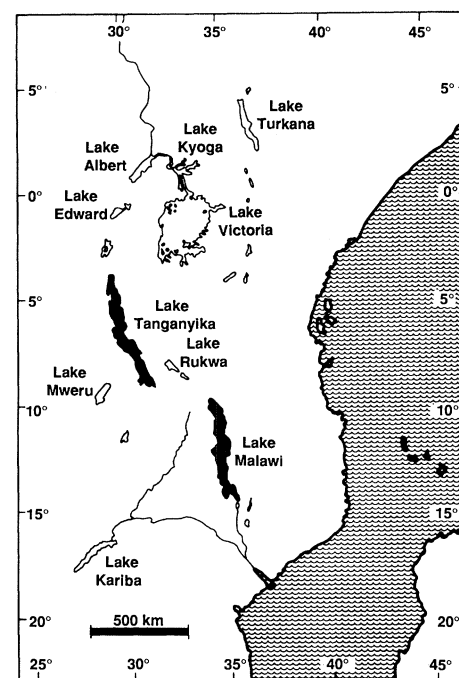


Fig. 1. The lakes of the East African rift system.

Project PROBE, Department of Geology, Duke University, Durham, NC 27706.